NANO LETTERS

pubs.acs.org/NanoLett Letter

Atomic-Resolution Mapping of Localized Phonon Modes at Grain Boundaries

Benedikt Haas,* Tara M. Boland, Christian Elsässer, Arunima K. Singh, Katia March, Juri Barthel, Christoph T. Koch, and Peter Rez

Cite This: *Nano Lett.* 2023, 23, 5975−5980 Read Online

ACCESS | Metrics & More | Article Recommendations | Supporting Information

ABSTRACT: Phonon scattering at grain boundaries (GBs) is significant in controlling the nanoscale device thermal conductivity. However, GBs could also act as waveguides for selected modes. To measure localized GB phonon modes, milli-electron volt (meV) energy resolution is needed with subnanometer spatial resolution. Using monochromated electron energy loss spectroscopy (EELS) in the scanning transmission electron microscope (STEM) we have mapped the 60 meV optic mode across GBs in silicon at atomic resolution and compared it to calculated phonon densities of states (DOS). The intensity is strongly reduced at GBs characterized by the presence of 5- and 7-fold rings where bond angles differ from the bulk. The excellent agreement between theory and experiment strongly supports the existence of localized phonon modes and thus of GBs acting as waveguides.

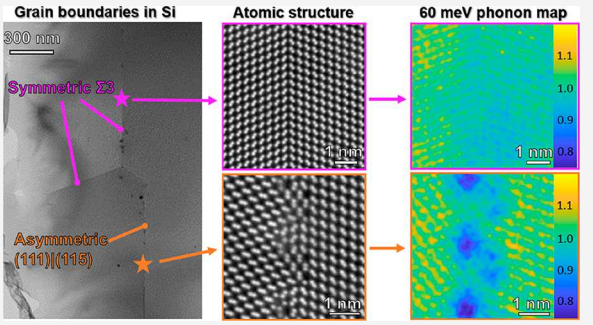

KEYWORDS: *scanning transmission electron microscopy, electron energy loss spectroscopy, semiconductors, phonons, grain boundaries, density functional theory*

Grain boundaries (GBs), the interfaces between crystallites that make up polycrystalline microstructures, control many materials properties. The scattering of phonons at GBs, especially localized modes, is significant for thermal conductivity at both the nanoscale and for polycrystals at the macroscale. In particular thermal conductivity at interfaces has been a significant problem for heat dissipation in nanoscale devices.[1] It is also critical for improving the performance of thermoelectrics that allow for the direct conversion of heat to electrical energy with no moving parts. The thermal conductivity is directly proportional to the phonon relaxation time, which is related to phonon scattering from defects. GBs predominately scatter low-frequency phonons that control thermal conductivity over critically important temperature ranges.[2,3]

Recently, there has also been interest in using phonons rather than photons for coherent coupling between mechanical oscillators, as a new paradigm for quantum sensing and information processing. Zivari et al. demonstrated phonon propagation in a single mode cavity waveguide fabricated in silicon.[4] Grain boundaries could act as waveguides that select particular localized phonon modes. These guided phonons could propagate further than in the bulk, thus opening up the possibility of building phononic devices. To detect and characterize such modes requires atomic resolution for the selected mode.

So far, investigations of GB effects on phonons have either been purely computational or used techniques such as Raman spectroscopy that lack the spatial resolution to detect individual vibrational modes at the GB. Developments in monochromated electron energy loss spectroscopy (EELS) in the scanning transmission electron microscope (STEM) have made it possible to probe phonon modes at the nanometer scale,[5] and even at atomic resolution in some well-chosen cases.[6,7] Hage et al. measured vibrational modes from a single silicon atom substituting for carbon in a graphene lattice.[8] Yan et al. showed the changes to vibrational spectra from a stacking fault in SiC[9] and Gadre et al. showed how the optic mode changes for sharp and diffuse interfaces between Ge and Si in a GeSi quantum dot, and related their observations to phonon dynamics.[10] Monochromated EELS in the STEM has also been used to probe how phonon modes change at heterointerfaces between diamond and hexagonal BN (hBN),[11] and Si and AlN.[12] Recently, Hoglund et al. reported changes in the optic mode spectra at different positions in a 10° boundary in strontium titanate, though not at atomic resolution.[13]

Received: March 21, 2023
Revised: June 14, 2023
Published: June 21, 2023

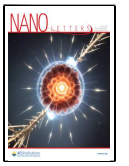

https://doi.org/10.1021/acs.nanolett.3c01089
Nano Lett. 2023, 23, 5975−5980

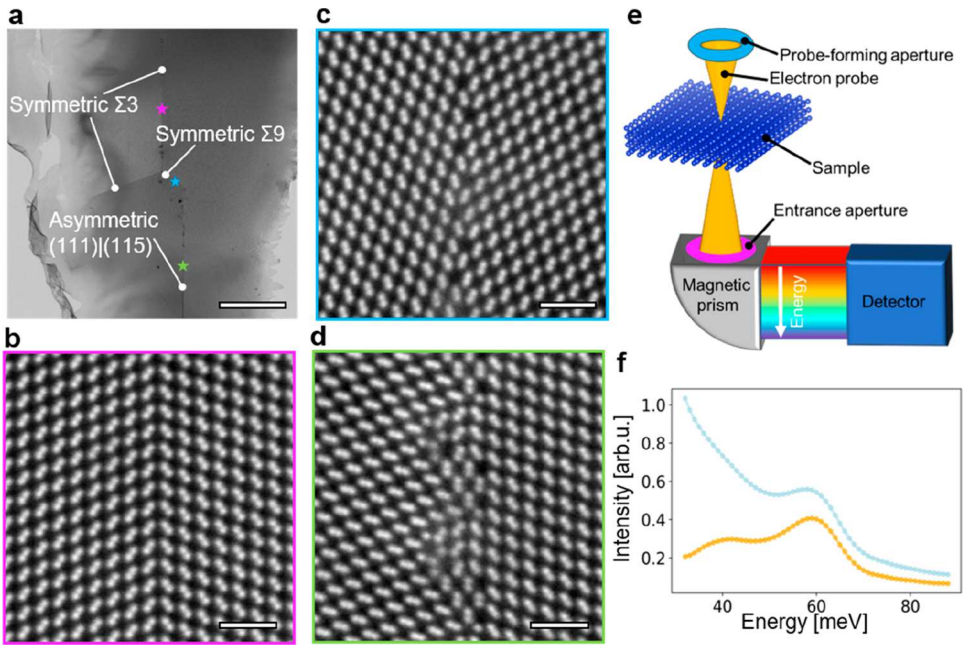

Figure 1. Structure of GBs and spectroscopy setup. (a) Overview bright-field image of the silicon sample showing the different GBs. Dark spots in the overview map stem from carbon contamination from previous experiments in a non-UHV microscope.[14] Scale bar: 500 nm. (b–d) high-resolution HAADF images of the Σ3 (111), symmetric Σ9 (221), and asymmetric (111)|(115) GBs, respectively. The positions of the acquisitions are marked in (a) as stars. Scale bars, 1 nm. (e) Experimental setup for the EELS measurements. (f) Experimental spectra from bulk silicon before (blue) and after (orange) background-subtraction, revealing the phonon signals at 40 and 60 meV.

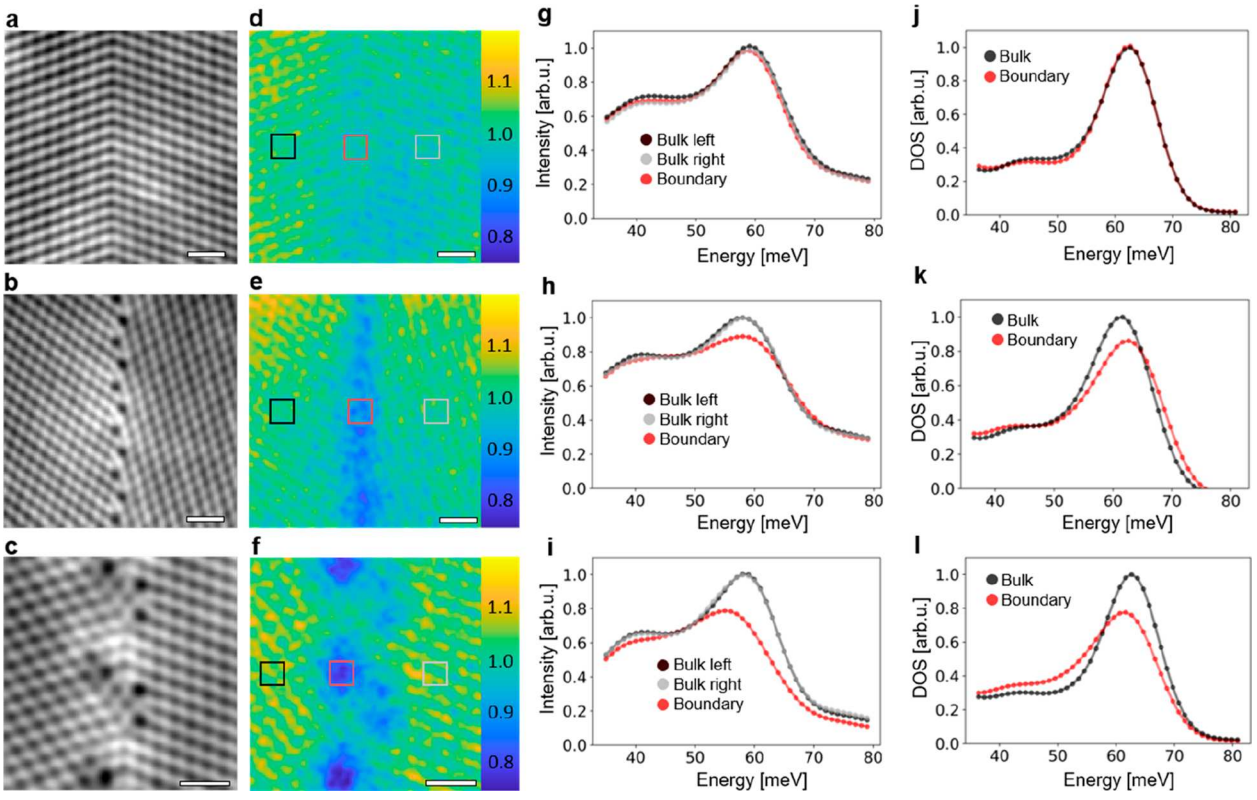

Figure 2. Comparison of experimental and calculated spectra for different GBs. (a–c) HAADF images acquired in parallel with spectrum maps of Σ3 (111), symmetric Σ9 (221), and asymmetric (111)|(115) GBs, respectively. Scale bars, 1 nm. (d–f) Maps of the amplitude of the 60 meV phonon peak, corresponding to the images in (a–c) respectively. Scale bars, 1 nm. (g–i) Spectra of bulk regions and from the GB for the three different GBs. (j–l) Calculated spectra for the three types of GBs.

Here, we demonstrate atomic-resolution phonon mapping of buried defects, in our case a symmetric Σ3 (111), a symmetric Σ9 (221) and an asymmetric (111)|(115) GB at a junction of three grains in a silicon polycrystal. The experimental spectra

https://doi.org/10.1021/acs.nanolett.3c01089
Nano Lett. 2023, 23, 5975−5980

are compared to simulated EELS spectra obtained from structure optimization of atomic models using molecular dynamics (MD) simulations and subsequent computation of the EELS spectra directly from the MD trajectories. For the Σ3 (111) GB, a model was built from high-resolution high-angle annular dark-field (HAADF) data acquired during the experiments, while for the symmetric Σ9 (221) and asymmetric (111)|(115) GBs, pre-existing models from literature are used (from Stoffers et al.[14] and Ziebarth et al.,[15] respectively) that were checked for consistency with the HAADF images.

Figure 1a is a low-magnification bright-field STEM image of a focused ion-beam prepared silicon sample in [$\bar{1}$10] orientation exhibiting the Σ3, Σ9, and (111)|(115) boundaries. Dark areas originate from carbon contamination that arose during previous experiments in a non-UHV microscope[14] and have been avoided in the present study. HAADF images acquired for the symmetric Σ3 (111), the symmetric Σ9 (221), and the asymmetric (111)|(115) GBs are depicted as Figure 1b–d, respectively, from the areas marked with stars in Figure 1a. A simplified diagram of the EELS experiments performed in a Nion HERMES STEM with an IRIS spectrometer is shown in Figure 1e. A convergent electron probe is focused on the sample and electrons scattered over a range of angles defined by the spectrometer entrance aperture are collected. These electrons are dispersed in energy by the prism of the spectrometer and recorded using a Dectris ELA direct electron detector. In our experiments the primary beam energy was 60 keV, the probe on the specimen had a 30 mrad convergence semiangle, and the spectrometer collection semiangle was 42 mrad. Further experimental parameters are given in the Supporting Information. A spectrum from bulk Si along [$\bar{1}$10] is shown in Figure 1f with the blue curve depicting the raw data and the orange one depicting the result after subtracting the zero-loss peak (ZLP), revealing the phonon signatures.

Since Si has two atoms in each primitive unit cell, it has both an optic and acoustic mode. However, there is no oscillating dipole that results in a spatially delocalized signal, because the two atoms are identical. Following Venkatraman et al.[7] and Gadre et al.,[10] it is then possible to collect the EELS signal on axis which results in a much stronger signal than would be collected with the displaced collection aperture required when dipole scattering is significant to not obscure atomic resolution through delocalization.[6]

The silicon optic mode with a relatively flat dispersion gives a peak in the density of states at about 60 meV and flat regions of the acoustic mode near the Brillouin zone boundaries result in a smaller peak at 40 meV.

Calculated phonon dispersion and densities of states (DOS) of phonons in crystals can be obtained by diagonalization of the dynamical matrix using force constants computed by methods of density functional theory (e.g., with the codes VASP[16] and Phonopy),[17] and the results agree well with experimental measurements.[17−19] However, this approach is computer-resource-intensive and is not practical for systems with large numbers of atoms, such as the supercells representing GB structures. Instead we take the Fourier transform of the velocity−velocity correlation function of MD trajectories computed using the Tersoff[20] empirical potential. It has been shown that this gives equivalent results, though the peaks are shifted to slightly higher energies with this empirical potential.[21]

Figure 2a–c shows HAADF images that were acquired in parallel with EELS maps of the Σ3 (111), symmetric Σ9 (221), and asymmetric (111)|(115) GBs, respectively. The change in appearance compared to the high-resolution HAADF images of Figure 1b–d stem from different experimental parameters (see the "Methods" section in the Supporting Information and Figure S1). In Figure 2d–f, the amplitude of the 60 meV peak is mapped out for the three GBs. In Figure 2g–i, spectra from the regions indicated by squares in Figure 2d–f for the GB and bulk on both sides are shown. While almost no variation is visible for the case of the Σ3 (111) GB, a clear dip in intensity is apparent for the symmetric Σ9 (221) GB which is even more pronounced for the asymmetric (111)|(115) GB. Variation of the phonon DOS is even clearly correlated with the structure along the boundary for the asymmetric (111)|(115) GB in the map. This correlation exists also for the Σ9 (221) GB, which can be better seen when extracting the averaged structural motif via template-matching (cf. Figure S2).

To ensure that indeed variations of the phonon DOS are mapped and not geometric effects due to being on or off an atomic column, the intensity of the peak around 40 meV was also investigated (see Figure S3). Since geometric effects would influence the relative intensity variations of the 40 meV peak in a similar manner, they can be ruled out.

Calculated phonon DOS that are derived from MD of structural models, based on or confirmed by the HAADF images in Figure 1b–d as mentioned above, are given in Figure 2j–k. Good agreement between the calculated and experimental spectra can be observed for the peak around 60 meV. Table 1 shows quantitative values for the height ratio and also the energy shift of the 60 meV peak for GB atoms relative to the same peak from bulk regions, shown as red and black boxes, respectively, in Figure 2d–f. The uncertainties were determined by measuring peak height and position over similar 10 × 10 pixel regions at different positions in the bulk (both sides of the GB were sampled) and calculating the standard deviation. The calculated depression of the 60 meV peak at the different boundaries is in excellent quantitative agreement with experimental results.

Table 1. Experimental and Calculated Height and Position of the 60 meV Peak for Different GBs in Si

GB type	exp. GB to bulk ratio	calc. GB to bulk ratio	exp. GB to bulk shift (meV)	calc. GB to bulk shift (meV)
Σ3 (111)	0.99 ± 0.03	1.01	(−0.3 ± 0.2)	−0.1
Σ9 (221)	0.89 ± 0.02	0.86	(0.0 ± 0.3)	+1.1
asymmetric (111)|(115)	0.79 ± 0.01	0.78	(−3.2 ± 0.2)	−1.3

The detailed theory for the intensity of features related to phonon scattering in STEM EELS is given by Rez and Singh[22] and Zeiger and Rusz.[23] It would seem that the dynamical diffraction of the probing and scattered electrons would have the same effect for spectra acquired from the boundary and bulk regions. For the position of the 60 meV peak, there is good agreement for Σ3 (111) and reasonable agreement for the asymmetric (111)|(115) GB, while for the symmetric Σ9 (221) GB a +1.1 meV shift is expected but none is observed. As discussed by Rez et al.,[21] any shifts could depend on the nature of the empirical potential so perfect agreement is not expected.

https://doi.org/10.1021/acs.nanolett.3c01089
Nano Lett. 2023, 23, 5975−5980

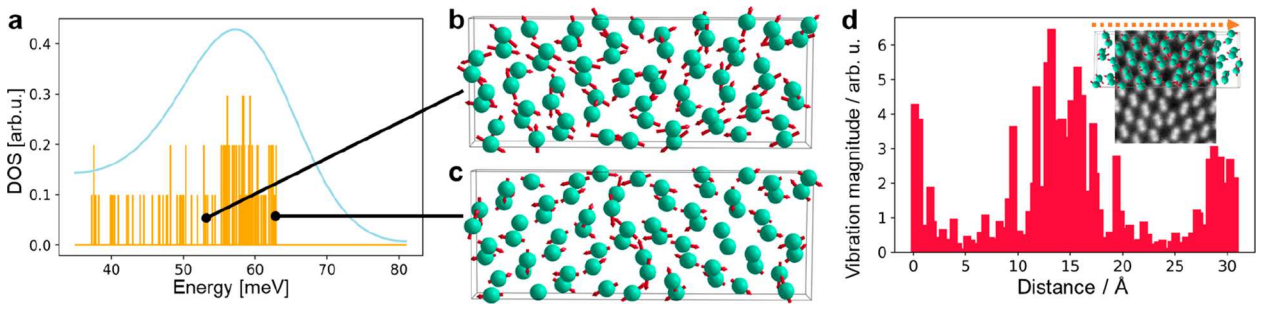

Figure 3. Ab-initio DOS and modes for Σ9 (221). (a) Calculated DOS for the Σ9 (221) GB as histogram plot (orange) and convolved with the experimental energy resolution (blue). (b) Super cell of the structure in the [110] direction (GB running from top to bottom in the center) with arrows representing the atom vibration direction and magnitude (exaggerated) of the bulk mode marked in the histogram in (a). (c) Visualization of a localized mode from the histogram in (a). (d) Profile of atomic vibration magnitudes across the GB in the super cell shown in (c) and summed perpendicular. The inset shows an overlay of (c) on top of an experimental HAADF image of the Σ9 (221) GB and the arrow indicates the profile direction.

The changes we observe are localized at individual atomic columns as shown in Figures 2, S2, and S3. The Σ9 (221) boundary has a 5- to 7-member ring pair per repeat distance, while the asymmetric GB has two. Although bond lengths are slightly changed in the 5- to 7-member rings, there are significant changes in the bond angles. As shown by Rez et al.[21] (Figure S2 in that article) this leads to a reduced amplitude of the displacements related to the 60 meV optic mode. Given that the bond lengths are minimally changed in the boundary region, it is not surprising that there are such small shifts in the peak energy. Furthermore, we see no evidence of peaks that might be due to interface states in the band gap in spectra from the boundary region (Figure S4). Recent reviews[24,25] show that since all boundary atoms are 4-fold coordinated, there should be no interface states at the boundary. The Σ3 boundary is coherent, a perfect twin, with the atomic structure unchanged right up to the boundary plane and thus produces virtually no modification of the phonon DOS. However, the same could be said for the stacking fault in 5H SiC investigated by Yan et al. where an enhancement of the acoustic mode intensity was observed when the probe was positioned at the stacking fault.[9] A more careful analysis shows that this fault was in fact a two-layer region of a different polytype, 3C SiC, and that the change in phonon DOS could therefore be explained by the difference in DOS between the two polytypes, so it is likely that these measurements are a consequence of a bulk property. It is interesting to note that the acoustic mode intensity at 40 meV is enhanced for some atoms on either side of the Σ9 (221) boundary plane as shown in Figure S3b.

The excellent agreement between experiment and simulation gives us high confidence in the predicted modes. Figure 3a depicts the DOS for the Σ9 (221) GB obtained from ab initio calculations. In Figure 3b, a typical bulk mode is depicted using arrows indicating the movement of each atom in the super cell of the calculation. A localized mode is shown in Figure 3c: Only the atoms constituting the boundary vibrate strongly, while the other (bulk) atoms exhibit negligible movement. It should be noted that the super cell exhibits a GB not only in the center but also at the left and right edges. To stress the localization of the mode, Figure 3d shows a profile of vibration magnitudes perpendicular to the GB and averaged along it with the inset showing the super cell overlaid to the HAADF image and the sketched profile direction. Large vibration amplitudes exist only where the GB atoms are located (center and both edges). As this mode is solely supported by the GB atoms, it should propagate with little damping. Therefore, the GB would act as a waveguide for such a localized mode, allowing it to be used in phononic devices.

We have demonstrated measurements of phonon DOS at atomic resolution at grain boundaries in silicon. Both from experimental STEM-EELS measurements and molecular-dynamics simulations, it could be established that changes in the optical phonon modes at GBs are associated with significant changes in bond angles (not lengths) as occurring in the 5- and 7-fold rings. Calculations of the relevant modes show that this arises from neighboring atom bonds that are no longer aligned. We expect that this will apply to similar materials, where measurements with high spatial resolution combined with high energy resolution will be more challenging. Our self-consistent scheme to determine and validate local DOS at the atomic scale by means of experiment and simulation should prove to be a powerful approach for the development of phononics.

■ ASSOCIATED CONTENT

Supporting Information

The Supporting Information is available free of charge at https://pubs.acs.org/doi/10.1021/acs.nanolett.3c01089.

Detailed methods and additional discussions of source-size broadening, energy resolution, robustness of EELS background fitting, sample thickness, extended spectra, surface oxidation, behavior of 40 meV peak, and supplementary references 1−14 (PDF)

■ AUTHOR INFORMATION

Corresponding Author

Benedikt Haas − *Department of Physics & IRIS Adlershof, Humboldt-Universität zu Berlin, 12489 Berlin, Germany;* orcid.org/0000-0002-9301-8511; Email: haas@physik.hu-berlin.de

Authors

Tara M. Boland − *School for Engineering of Matter Transport and Energy, Arizona State University, Tempe, Arizona 85287-6106, United States;* Present Address: Computational Atomic-Scale Materials Design (CAMD), Technical University of Denmark; Kgs. Lyngby, 2800, Denmark

Christian Elsässer − *Fraunhofer Institute for Mechanics of Materials IWM, 79108 Freiburg, Germany*

https://doi.org/10.1021/acs.nanolett.3c01089
Nano Lett. 2023, 23, 5975−5980

Arunima K. Singh − *Department of Physics, Arizona State University, Tempe, Arizona 85287-1504, United States;* orcid.org/0000-0002-7212-6310
Katia March − *Sorbonne Université, Muséum National d'Histoire Naturelle, UMR CNRS 7590, Institut de Minéralogie, de Physique des Matériaux et de Cosmochimie, IMPMC, 75005 Paris, France*
Juri Barthel − *Ernst Ruska-Centre (ER-C 2), Forschungszentrum Jülich, 52428 Jülich, Germany;* orcid.org/0000-0003-3914-4346
Christoph T. Koch − *Department of Physics & IRIS Adlershof, Humboldt-Universität zu Berlin, 12489 Berlin, Germany;* orcid.org/0000-0002-3984-1523
Peter Rez − *Department of Physics, Arizona State University, Tempe, Arizona 85287-1504, United States;* orcid.org/0000-0003-3424-9042

Complete contact information is available at: https://pubs.acs.org/10.1021/acs.nanolett.3c01089

Author Contributions

P.R. conceived the study. B.H. conducted the experiments, and B.H and P.R. performed the data analysis. T.M.B. performed structure model pre-/processing, and T.M.B., P.R., C.E., and A.S. performed the theoretical calculations. K.M. performed preliminary experiments. C.T.K. built the atomistic GB models from experimental HAADF-STEM images. C.E. provided some preinvestigated atomistic GB models. J.B. contributed the preinvestigated silicon sample. B.H. and P.R. wrote the manuscript. All authors contributed to and approved the final draft of the manuscript.

Notes

The authors declare no competing financial interest.

■ ACKNOWLEDGMENTS

T.B. and A.S. are supported in part by the Arizona State University start-up funds. A.S. is also funded by the NSF DMR under Grant No. 1906030 and as part of ULTRA, an Energy Frontier Research Center funded by the U.S. Department of Energy (DOE), Office of Science, Basic Energy Sciences (BES), under Award No. DE-SC0021230. The MD simulations were performed using the Extreme Science and Engineering Discovery Environment (XSEDE), supported by National Science Foundation grant number TG-DMR150006; the HPC resources from Research Computing at Arizona State University; and the National Energy Research Scientific Computing Center, a DOE Office of Science User Facility supported by the Office of Science of the U.S. Department of Energy under Contract No. DE-AC02-05CH11231. The authors thank Ondrej L. Krivanek and Andrea Konečná for critical reading of the manuscript.

■ REFERENCES

(1) Cahill, D. G.; Ford, W. K.; Goodson, K. E.; Mahan, G. D.; Majumdar, A.; Maris, H. J.; Merlin, R.; Phillpot, S. R. Nanoscale thermal transport. *J. Appl. Phys.* **2003**, *93* (2), 793−818.
(2) Cheng, Z.; Li, R.; Yan, X.; Jernigan, G.; Shi, J.; Liao, M. E.; Hines, N. J.; Gadre, C. A.; Idrobo, J. C.; Lee, E.; et al. Experimental observation of localized interfacial phonon modes. *Nat. Commun.* **2021**, *12* (1), 6901.
(3) Kim, S. I.; Lee, K. H.; Mun, H. A.; Kim, H. S.; Hwang, S. W.; Roh, J. W.; Yang, D. J.; Shin, W. H.; Li, X. S.; Lee, Y. H.; et al. Thermoelectrics. Dense dislocation arrays embedded in grain boundaries for high-performance bulk thermoelectrics. *Science* **2015**, *348* (6230), 109−114.
(4) Zivari, A.; Stockill, R.; Fiaschi, N.; Gröblacher, S. Non-classical mechanical states guided in a phononic waveguide. *Nature Physics* **2022**, *18* (7), 789−793.
(5) Krivanek, O. L.; Lovejoy, T. C.; Dellby, N.; Aoki, T.; Carpenter, R. W.; Rez, P.; Soignard, E.; Zhu, J. T.; Batson, P. E.; Lagos, M. J.; et al. Vibrational spectroscopy in the electron microscope. *Nature* **2014**, *514* (7521), 209−214.
(6) Hage, F.; Kepaptsoglou, D. M.; Ramasse, Q. M.; Allen, L. J. Phonon Spectroscopy at Atomic Resolution. *Phys. Rev. Lett.* **2019**, *122* (1), 016103.
(7) Venkatraman, K.; Levin, B. D. A.; March, K.; Rez, P.; Crozier, P. A. Vibrational spectroscopy at atomic resolution with electron impact scattering. *Nature Physics* **2019**, *15* (12), 1237−1241.
(8) Hage, F. S.; Radtke, G.; Kepaptsoglou, D. M.; Lazzeri, M.; Ramasse, Q. M. Single-atom vibrational spectroscopy in the scanning transmission electron microscope. *Science* **2020**, *367* (6482), 1124−1127.
(9) Yan, X.; Liu, C.; Gadre, C. A.; Gu, L.; Aoki, T.; Lovejoy, T. C.; Dellby, N.; Krivanek, O. L.; Schlom, D. G.; Wu, R.; et al. Single-defect phonons imaged by electron microscopy. *Nature* **2021**, *589* (7840), 65−69.
(10) Gadre, C. A.; Yan, X.; Song, Q.; Li, J.; Gu, L.; Huyan, H.; Aoki, T.; Lee, S. W.; Chen, G.; Wu, R.; et al. Nanoscale imaging of phonon dynamics by electron microscopy. *Nature* **2022**, *606* (7913), 292−297.
(11) Qi, R.; Shi, R.; Li, Y.; Sun, Y.; Wu, M.; Li, N.; Du, J.; Liu, K.; Chen, C.; Chen, J.; et al. Measuring phonon dispersion at an interface. *Nature* **2021**, *599* (7885), 399−403.
(12) Li, Y. H.; Qi, R. S.; Shi, R. C.; Hu, J. N.; Liu, Z. T.; Sun, Y. W.; Li, M. Q.; Li, N.; Song, C. L.; Wang, L. Atomic-scale probing of heterointerface phonon bridges in nitride semiconductor. *Proc. Natl. Acad. Sci. U S A* **2022**, *119* (8), e2117027119.
(13) Hoglund, E. R.; Bao, D. L.; O'Hara, A.; Pfeifer, T. W.; Hoque, M. S. B.; Makarem, S.; Howe, J. M.; Pantelides, S. T.; Hopkins, P. E.; Hachtel, J. A. Direct Visualization of Localized Vibrations At Complex Grain Boundaries. *Adv. Mater.* **2023**, *35*, No. e2208920.
(14) Stoffers, A.; Ziebarth, B.; Barthel, J.; Cojocaru-Miredin, O.; Elsässer, C.; Raabe, D. Complex Nanotwin Substructure of an Asymmetric Sigma9 Tilt Grain Boundary in a Silicon Polycrystal. *Phys. Rev. Lett.* **2015**, *115* (23), 235502.
(15) Ziebarth, B.; Mrovec, M.; Elsässer, C.; Gumbsch, P. Interstitial iron impurities at grain boundaries in silicon: A first-principles study. *Phys. Rev. B* **2015**, *91* (3), 035309.
(16) Kresse, G.; Furthmüller, J. Efficient iterative schemes for ab initio total-energy calculations using a plane-wave basis set. *Phys. Rev. B* **1996**, *54* (16), 11169−11186.
(17) Togo, A.; Tanaka, I. First principles phonon calculations in materials science. *Scripta Materialia* **2015**, *108*, 1−5.
(18) Frank, W.; Elsässer, C.; Fähnle, M. Ab initio Force-Constant Method for Phonon Dispersions in Alkali Metals. *Phys. Rev. Lett.* **1995**, *74* (10), 1791−1794.
(19) Kresse, G.; Furthmüller, J.; Hafner, J. Ab initio Force Constant Approach to Phonon Dispersion Relations of Diamond and Graphite. *Europhysics Letters (EPL)* **1995**, *32* (9), 729−734.
(20) Tersoff, J. Modeling solid-state chemistry: Interatomic potentials for multicomponent systems. *Phys. Rev. B Condens. Matter.* **1989**, *39* (8), 5566−5568.
(21) Rez, P.; Boland, T.; Elsässer, C.; Singh, A. Localized Phonon Densities of States at Grain Boundaries in Silicon. *Microsc. Microanal.* **2022**, *28* (3), 672−679.
(22) Rez, P.; Singh, A. Lattice resolution of vibrational modes in the electron microscope. *Ultramicroscopy* **2021**, *220*, 113162.
(23) Zeiger, P. M.; Rusz, J. Efficient and Versatile Model for Vibrational STEM-EELS. *Phys. Rev. Lett.* **2020**, *124* (2), 025501.
(24) Sun, L.; Marques, M. A. L.; Botti, S. Direct insight into the structure-property relation of interfaces from constrained crystal structure prediction. *Nat. Commun.* **2021**, *12* (1), 811.

(25) Kohyama, M. Computational studies of grain boundaries in covalent materials. *Modelling and Simulation in Materials Science and Engineering* **2002**, *10* (3), R31−R59.

https://doi.org/10.1021/acs.nanolett.3c01089
Nano Lett. 2023, 23, 5975−5980